Journal of
Renewable Energy Research and Applications (RERA)

*Vol 2. No 1, 2021, 137-146* *DOI: 10.22044/RERA.2021.10694.1053*

# Two-level DPC Strategy Based on FNN Algorithm of DFIG-DRWT Systems Using Two-level Hysteresis Controllers for Reactive and Active Powers

Benbouhenni Habib

*Labo. LAAS, Departement de Génie Electrique, Ecole Nationale Polytechnique d'Oran Maurice Audin, Oran, Algeria.*

Received Date 07 April 2021; Revised Data 27 April 2021 Accepted Date 03 May 2021
*Corresponding author:habib_benbouhenni@yahoo.com (B. Habib)*

**Abstract**
In this paper, a novel switching table (ST) of the twelve sectors direct power command (DPC) strategy of doubly-fed induction generator (DFIG)-based dual rotor wind power (DRWP) is proposed using two-level hysteresis controllers for the reactive and active power and feedforward neural networks (FNNs) algorithms. This intelligent technique is used to replace the conventional ST in order to reduce the rotor flux ripple, active power ripple, total harmonic distortion (THD) of stator voltage, torque, and reactive power undulations. The simulation and modeling of the proposed strategy are carried out in the Matlab software. DFIG is tested in association with the DRWP system. The simulation results obtained show that DPC with FNN controller (DPC-FNN) reduce the THD values of the stator voltage, rotor flux undulation, active/reactive power undulation, and electromagnetic torque ripple compared to the conventional DPC strategy. According to the results obtained, the current waveform becomes purely sinusoidal with a reduction in the THD rate to 0.64%.

**Keywords:** *DPC, DFIG, ST, THD, FNNs, DPC-FNN, DRWP.*

## 1. Introduction

Nowadays, the three-phase DFIGs are widely used in wind power due to their low maintenance requirement and simple form. Several techniques have been tried to command DFIGs. For years, the DFIG command market has been dominated by the field-oriented command (FOC) techniques [1]. However, the latest trend is the development of the direct power command (DPC) since it is a fast, simple, and robust technique [2]. The DPC technique gives a fast dynamic reactive power (Qs) and an active power (Ps) response. The DPC technique uses two hysteresis comparators and one switching table [3, 4]

The DPC strategy is a fast control of DFIG. However, this technique gives more ripples in the stator voltage, torque, rotor flux, reactive power, stator current, and active power. On the other hand, the classical DPC technique with a swithing table gives a more THD value for the stator voltage. A novel DPC technique has been proposed based on a seven-level space vector pulse width modulation (7L-SVPWM) strategy, where the hysteresis controllers (HCs) are replaced by two proportional-integral (PI) controllers and the lookup table by the 7L-SVPWM strategy. This proposed DPC technique reduced more and more the THD values of the stator voltage and ripples in the active power, torque, rotor current, reactive power compared to the traditional DPC and field-oriented control strategy of DFIG [5]. The DPC method has been proposed based on the discrete SVPWM in order to reduce the reactive and active power of a DFIG [6]. The direct torque control (DTC) of DFIG gives better performances compared to the DPC method because the DTC methods control the torque directly [7].

In the recent years, the feedforward neural networks (FNNs) technique has been widely used to control the AC machines. The neural networks are controlled based on the observations and engineering experience. On the other hand, this technique has attracted a lot of research works on command for the last two decades. It is a simple technique and is easy to implement compared to the classical strategies [4]. In the neural algorithm, an exact mathematical model is not necessary because the layers are used to define the system behavior rapidly.

The FNN controller has been applied to the induction motor (IM) control, and it has been presented in [8, 9]. In this control schemes, the switching table is based on the FNN controller to minimize the torque ripple and flux ripple. In [10], the author has proposed a novel DTC technique based on the FNN algorithm of permanent magnet synchronous motor (PMSM). In this new DTC control, the lookup table and the proportional-integral (PI) controller of speed are replaced by the FNN controllers. This novel strategy is a simple method, and has minimized the electromagnetic torque compared to the classical DTC control. The sliding mode controller (SMC) and FNN strategy are combined to command DFIG [11]. In [12], the two hysteresis comparators of DTC for IM are proposed based on the FNN controllers. In [13], a second-order sliding mode control (SOSMC) based on the FNN technique has been proposed in order to minimize the stator current and torque ripples of DFIG. The neural SVPWM strategy has been proposed to command the converter of DFIG controlled by the direct vector control [14, 15]. In [16], an neural SMC strategy (NSMC) has been designed to command DFIG using the neural PWM strategy. In [17], the neural PI controllers and the SVPWM technique have been combined to minimize the torque ripple of the DFIG-based wind turbine. In [18], a new SVPWM technique has been proposed based on the FNN method of permanent magnet synchronous generator (PMSG) controlled by the DPC strategy. In [19], the super-twisting sliding mode (STSM) algorithm has been proposed based on the FNN technique in order to control DFIG using the DTC strategy. In [20], the author has proposed the control strategies based on the FNN technique for PMSG-WT. The two command schemes are DTC and the DPC strategy. The DPC method has been proposed based on the feedforward neural hysteresis comparators (FNHC) in order to minimize THD of the stator voltage of DFIG [21].

In this work, the twelve sectors DPC (TSDPC) system with the application of feedforward neural network (FNN) algorithm is considered. The original contribution of this work is the application of the FNN algorithm in the TSDPC system with the DFIG and simulation investigation of this new control strategy.

In this paper, the sensorless TSDPC strategy will be introduced. First, we will illustrate the traditional TSDPC strategy. Then the concept of reactive power ripple minimizetion technique will be discussed. The classical switching table, feedforward neural switching table (FNST), and the scheme will be presented. The effectiveness of the proposed twetve-sector DPC method is compared to the classical DPC strategy using the Matlab logiciel.

## 2. TSDPC with two-level HCs

The basic principle of DPC, proposed by Noguchi, is based on the DTC method [22]. In the classical DPC strategy, a 3-level HC is used for Ps and a 2-level HC for Qs. In addition, the position of the rotor flux is a six region command (1, 2, 3, 4, 5, 6) [23]. In this section, The TSDPC method with two-level hysteresis comparators is a modification of the classical DPC technique with 6 sectors, where the three-level HC of active power has been replaced by two-level hysteresis comparator. In this proposed strategy, the position of the rotor flux is a twelve region control (N = 1, 2,…,12). This proposed method is a robust strategy, easy to implement, and robust compared to the traditional DPC strategy. The proposed ST of TSDPC is shown in Table 1. In addition, the TSDPC strategy of DFIG-DRWP with the application of the two-level hysteresis controllers is shown in Figure 1. On the other hand, the principal of DRWP is detailed in [24, 25].

The rotor flux can be estimated by [26]:

$$\begin{cases} \Psi_{\alpha r} = \int_0^t (-R_r I_{\alpha r} + V_{\alpha r})dt \\ \Psi_{\beta r} = \int_0^t (-R_r I_{\beta r} + V_{\beta r})dt \end{cases} \quad (1)$$

With:

$$\psi_r = \sqrt{\Psi_{\alpha r}^2 + \Psi_{\beta r}^2} \quad (2)$$

The angle of rotor flux is calculated by:

$$\theta_r = arctg(\frac{\Psi_{\beta r}}{\Psi_{\alpha r}}) \quad (3)$$

The active and reactive powers are estimated using (4) and (5).

$$P_s = -\frac{3}{2}\frac{L_m}{\sigma.L_s.L_r}\cdot(V_s.\psi_{\beta r}) \quad (4)$$

$$Q_s = -\frac{3}{2}(\frac{V_s}{\sigma.L_s}\cdot\psi_{\beta r} - \frac{V_s.L_m}{\sigma.L_s.L_r}\cdot\psi_{\alpha r}) \quad (5)$$

With

$$\Psi_{\alpha r} = \sigma L_r I_{\alpha r} + \frac{M}{L_s}\Psi_s \quad (6)$$

$$\Psi_{\beta r} = \sigma L_r I_{\beta r} \quad (7)$$

$$\left|\overline{V_s}\right| = \left|\overline{\Psi_s}\right|.w_s \quad (8)$$

$$\sigma = 1 - \frac{M^2}{L_r L_s} \quad (9)$$

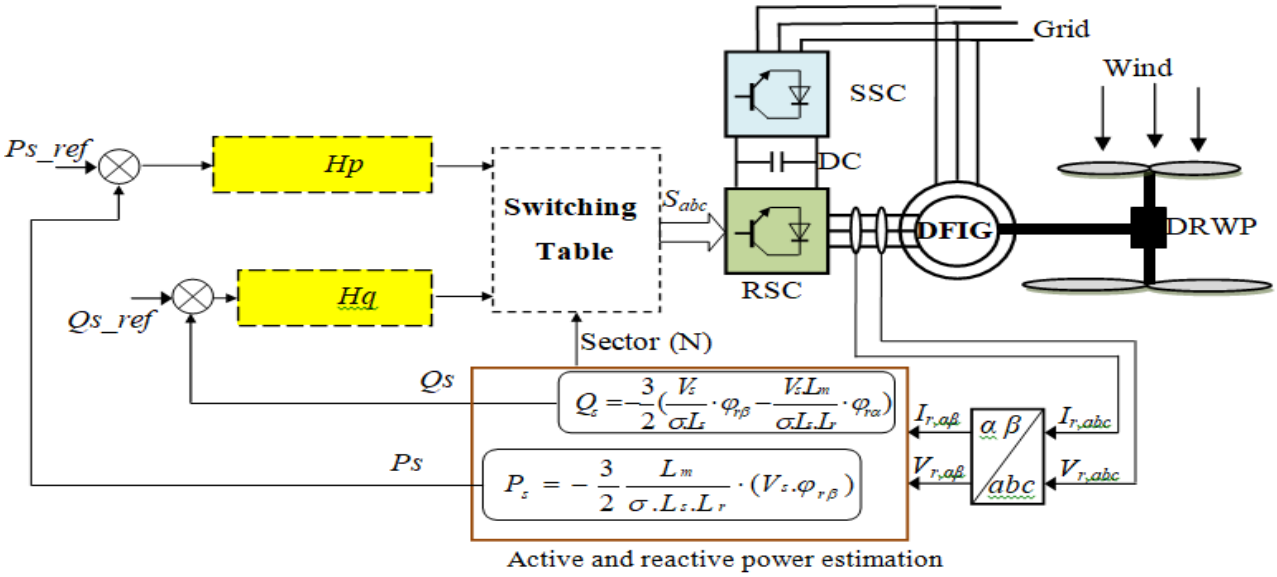


**Figure 1. TSDPC control scheme**

**Table 1. Proposed lookup table of the 12-sector DPC strategy.**

| N | Hq | | | |
|---|---|---|---|---|
| | 1 | | 0 | |
| | Hp | | | |
| | 1 | 0 | 1 | 0 |
| 1 | 1 | 6 | 3 | 5 |
| 2 | 1 | 6 | 3 | 5 |
| 3 | 2 | 1 | 4 | 6 |
| 4 | 2 | 1 | 4 | 6 |
| 5 | 3 | 2 | 5 | 1 |
| 6 | 3 | 2 | 5 | 1 |
| 7 | 4 | 3 | 6 | 2 |
| 8 | 4 | 3 | 6 | 2 |
| 9 | 5 | 4 | 1 | 3 |
| 10 | 5 | 4 | 1 | 3 |
| 11 | 6 | 5 | 2 | 4 |
| 12 | 6 | 5 | 2 | 4 |

Figure 2 and Figure 3 show the hysteresis controllers of the active and reactive powers for DFIG-DRWP controlled by the TSDPC strategy, respectively. These controllers are simple algorithms and are easy to be applied. On the other hand, these controllers do not require the mathematical model of the system.

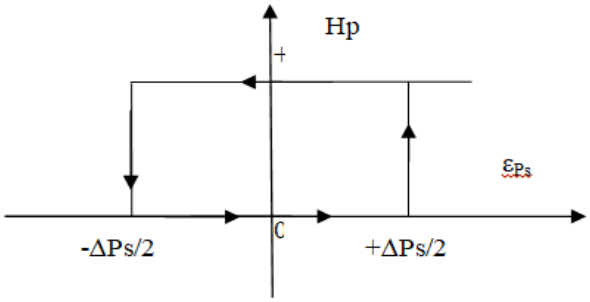


**Figure 2. Active power hysteresis controller.**

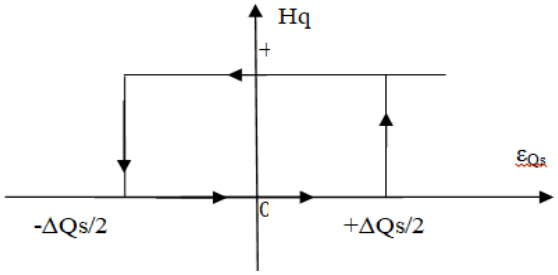


**Figure 3. Reactive power hysteresis controller.**

## 3. TSDPC strategy with FNN algorithm

In order to improve the TSDPC performance, the complimentary use of the FNN algorithm is proposed. The principle of TSDPC with the FNN algorithm (TSDPC-FNN) is similar to the TSDPC control scheme. The difference is using the FNN technique in order to replace the lookup table. The graphical representation of the TSDPC strategy with the FNN controller is shown in Figure 4. This proposed technique minimize the active power undulation, reactive power undulation, and THD of the stator voltage of DFIG-DRWP compared to the TSDPC and DPC strategies. This proposed TSDPC method is a robust one, has a simple structure, and is easy to implement.

The recent applications of the FNN strategy have become more convenient in the control systems. The FNN strategy is popular in more applications. Since robustness is the best advantage of an FNN technique, it has been widely employed to command the AC machines. There are many models of feedforward neural networks. Among the most famous of them is the back-propagation neural network algorithm proposed in 1986 [27].

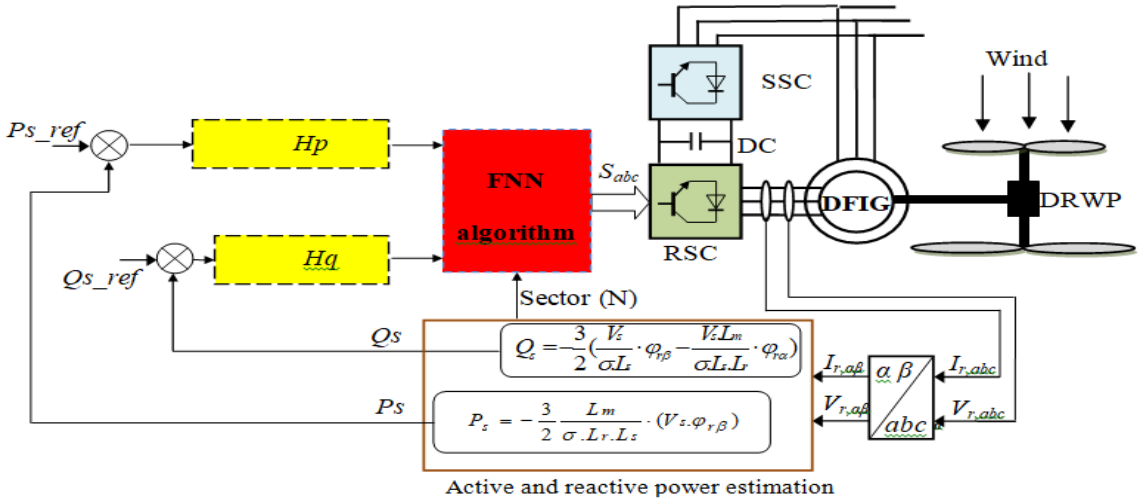


**Figure 4. TSDPC control scheme with FNN algorithm.**

This suggested neural algorithm has become one of the most widely used neural models in control of the AC machine drive. The neural controller contains three layer: hidden layer, output layer, and input layer. On the other hand, the training algorithm proposed in this paper is the retro-propagation of Levenberg-Marquardt (LM). This algorithm is simple to use. The parameters of the LM algorithm are shown in Table 2.

**Table 2. LM algorithm.**

| Parameters | Values |
|---|---|
| TrainParam.goal | 0 |
| TrainParam.Lr | 0.002 |
| Number of output layers | 3 |
| TrainParam.mu | 0.9 |
| TrainParam.show | 50 |
| TrainParam.eposh | 500 |
| Number of hidden layers | 1 |
| Number of neurones in hidden layer | 10 |
| Coeff. of acceleration of convergence (mc) | 0.9 |
| Number of input layers | 3 |
| Functions of activation | Purling, Tensing, gensim |

An automatic learning of the FNN controller is performed until a small squared error of 2.173× $10^{-9}$ is obtained (see Figure 5). It should be noted that this small error is obtained after 406 iterations.

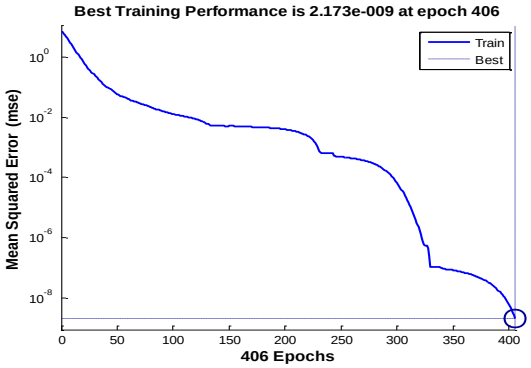


**Figure 5. Learning of the FNN controller.**

The FNN structure used for the switching table is illustrated in Figure 6. Figure 7 shows layer 1 of the FNN controllers. On the other hand, Figures 8 and 9 show the hidden layer and layer 2, respectively.

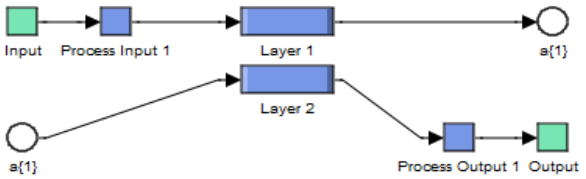


**Figure 6. Block diagram of the FNN controller.**

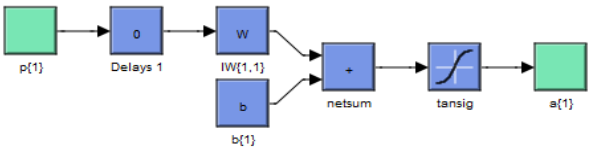


**Figure 7. Block diagram of layer 1.**

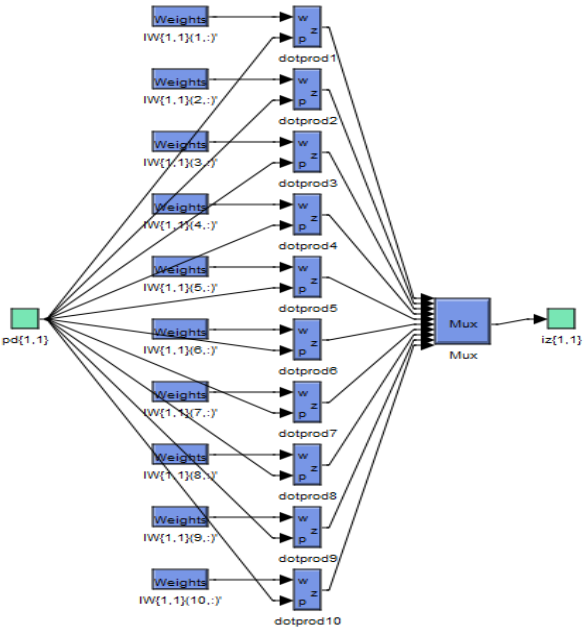


**Figure 8. Hidden layer.**

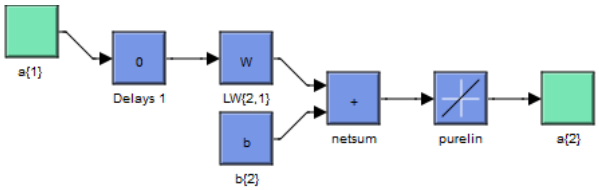


**Figure 9. Layer 2.**

## 4. Results and discussion

Simulations of TSDPC and TSDPC with FNN controllers for a DFIG-DRWP are carried out using the Matlab. The DFIG parameters are shown in Table 3. The performance analysis is done with the stator reactive power, THD value of stator current, and stator active power.

**Table 3. DFIG-DRWP parameters [28, 29].**

| | |
|---|---|
| Pn | 1.5 MW |
| Ω | 150 rad/s |
| P | 2 |
| Vn | 380V |
| Rr | 0.021Ω |
| Lr | 0.0136H |
| Lm | 0.0135H |
| Rs | 0.012Ω |
| Ls | 0.0137H |
| Fr | 0.0024Nm.s/rad |
| J | 1000 Kg.m$^2$ |
| f | 50 Hz |
| $P_{DRWT}$ | 1.5 MW |
| $d_M$ | 51 m |
| $d_A$ | 26.4 m |

### 4.1 Reference tracking test (RTT)

In this part, Qs and Ps track almost perfectly their reference values (Figures 12, 13). The TSDPC-FNN technique minimized Ps and Qs compared to the TSDPC control scheme (Figures 14, 15). Figures 10 and 11 show the THD value of current for the TSDPC-FNN and TSDPC control one, respectively. It can be clearly observed that the THD value is reduced for the TSDPC-FNN technique (0.32 %) when compared to TSDPC (0.91%). It is clear from the results obtained that TSDPC-FNN has satisfied performance. In addition, this proposed technique minimized the THD value of the stator current compared to the VFDPC (virtual flux direct power control) strategy (see Table 4) and field oriented control (see Ref. [30] and Ref. [31]).

The TSDPC-FNN technique minimized the time response of the reactive power (tr = 0.58 ms) when compared to TSDPC (tr = 0.94 ms).

**Table 4. THD value (RTT).**

| | | THD (%) |
|---|---|---|
| **Ref. [30]** | **DPC** | 4.88 |
| | **VFDPC** | 4.19 |
| **Ref. [31]** | | 3.7 |
| **Proposed methods** | **TSDPC** | 0.91 |
| | **TSDPC-FNN** | 0.32 |

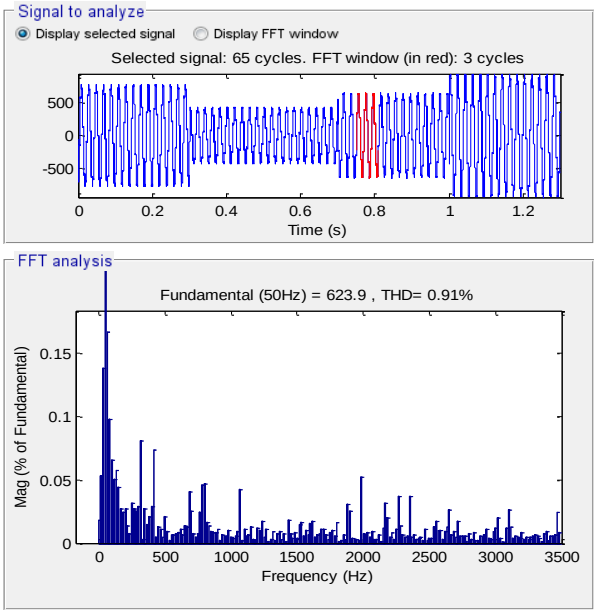


**Figure 10. Harmonic distortion (TSDPC).**

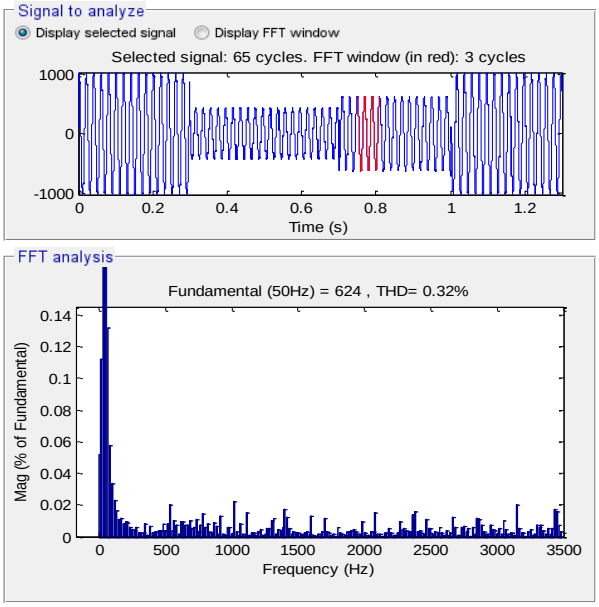


**Figure 11. Harmonic distortion (TSDPC-FNN).**

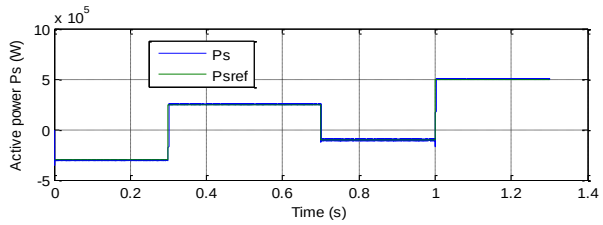


**a) TSDPC**

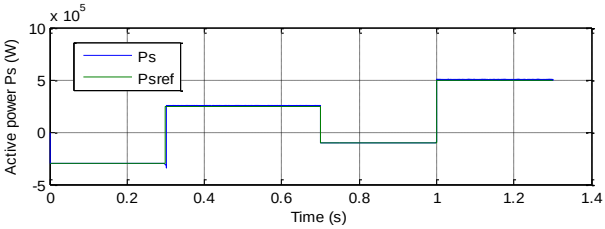


**b) TSDPC-FNN**

**Figure 12. Active power (RTT).**

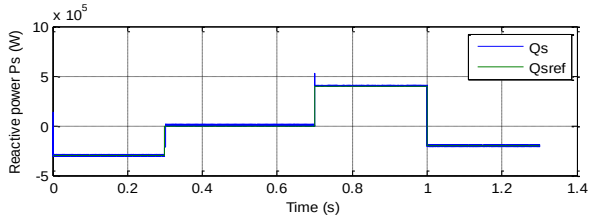


**a) TSDPC**

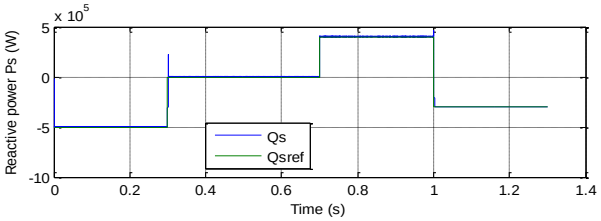


**b) TSDPC-FNN**

**Figure 13. Reactive power (RTT).**

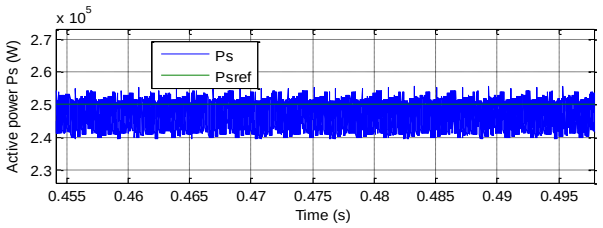


**a) TSDPC**

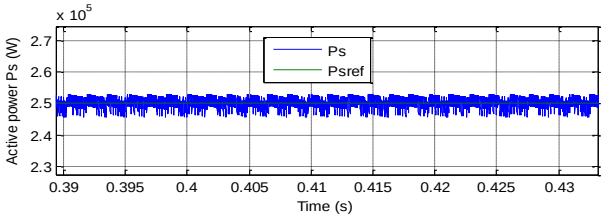


**b) TSDPC-FNN**

**Figure 14. Zoom in the active power (RTT).**

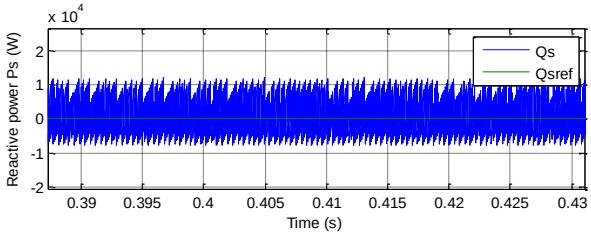


**a) TSDPC**

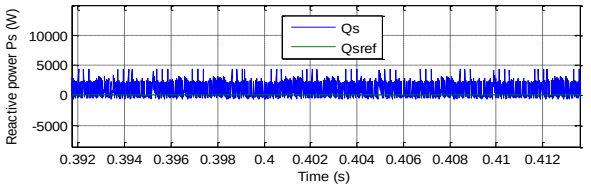


**b) TSDPC-FNN**

**Figure 15. Zoom in the reactive power (RTT).**

## 4.2. Robustness test (RT)

In this test, the values of $R_s$ and $R_r$ are multiplied by 2 and the values of $L_s$ and $L_r$ are multiplied by 0,5. The simulation results are presented in Figs. 16-21. As it has been shown in these figures, these variations present a clear effect on the active power (see Figure 18), THD value of current (see Figures 19, 20), and stator reactive power (see Figure 19), and that the effect appears more important for the classical TSDPC control than that with the TSDPC-FNN control scheme. The proposed DPC technique minimized the THD value compared to DPC with the neural STSM method (DPC-NSTSM) [32], DPC with three-level NPC inverter [33], DPC with three-level NSVPWM technique [34], direct vector control with three-level NSVPWM technique, and fuzzy SMC based on the three-level SVPWM strategy [35] (See Table 5).

**Table 5. THD value (RT)**

| | | THD(%) |
|---|---|---|
| **Ref. [32]** | **DPCPI** | 4.84 |
| | **DPC-NSTSM** | 2.98 |
| **Ref. [33]** | **Classical DPC** | 1.74 |
| | **DPC-NPC** | 0.96 |
| **Ref. [34]** | **Classical DPC** | 2.75 |
| | **DPC-3L-NSVPWM** | 0.77 |
| **Ref. [35]** | **DVC-3L-SVPWM** | 7.55 |
| | **FSMC-3LSVPWM** | 0.52 |
| **Proposed methods** | **TSDPC** | 2.04 |
| | **TSDPC-FNN** | 0.32 |

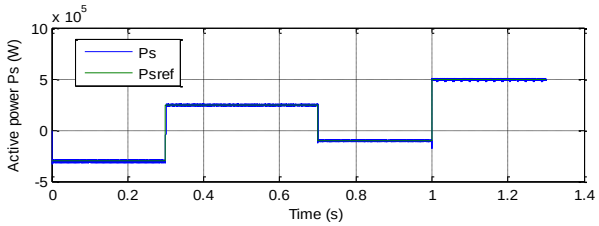


**a) TSDPC**

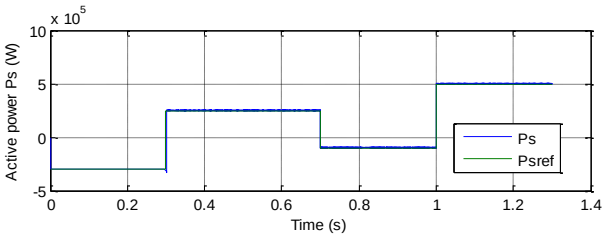


**b) TSDPC-FNN**

**Figure 16. Active power (RT).**

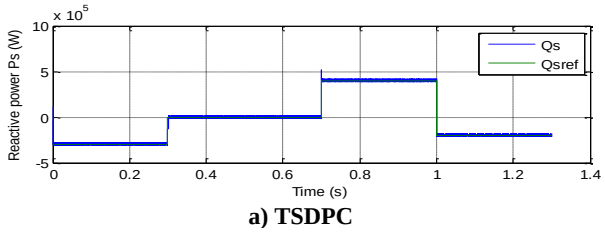


**a) TSDPC**

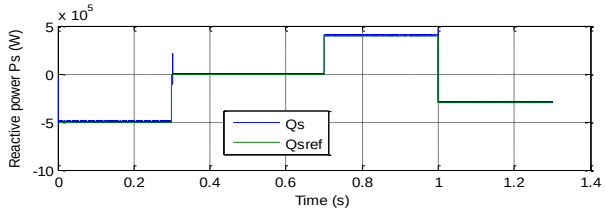


**b) TSDPC-FNN**

**Figure 17. Reactive power (RT).**

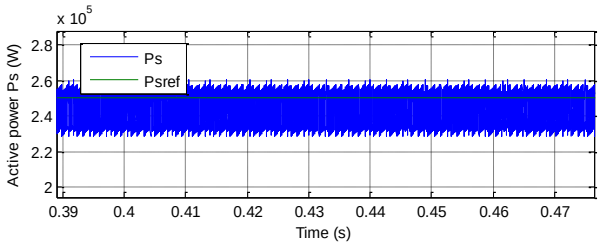


**a) TSDPC**

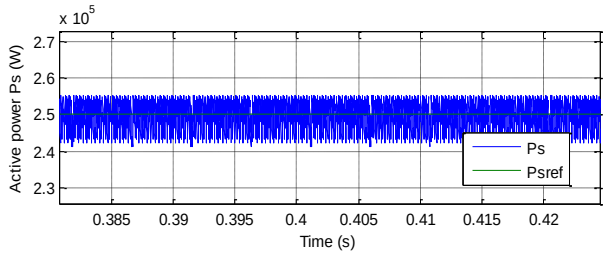


**b) TSDPC-FNN**

**Figure 18. Zoom in Ps (RT).**

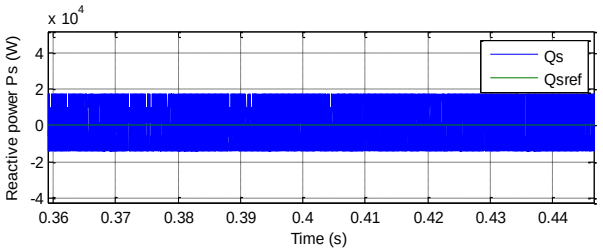


**a) TSDPC**

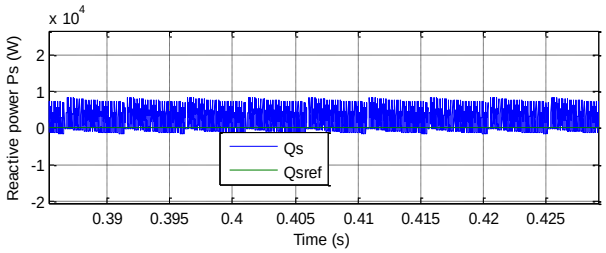


**b) TSDPC-FNN**

**Figure 19. Zoom in Qs (RT).**

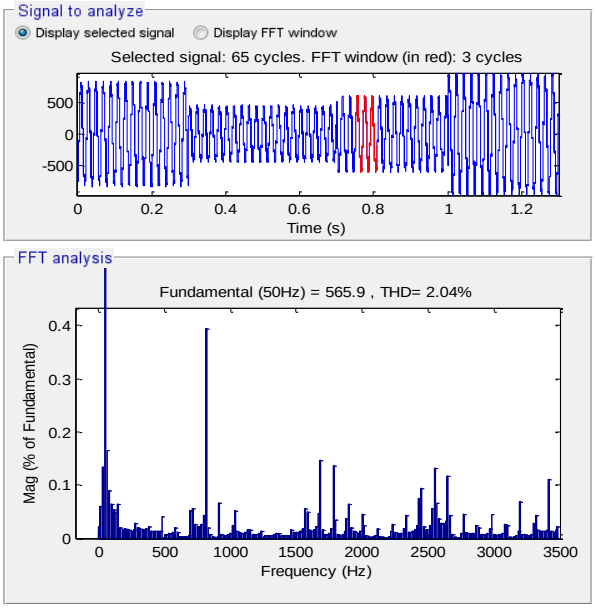


**Figure 20. Harmonic distortion (TSDPC).**

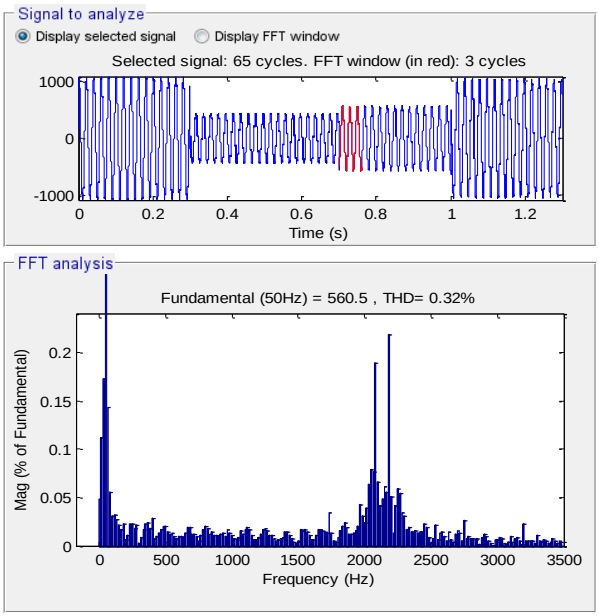


**Figure 21. Harmonic distortion (TSDPC-FNN).**

## 5. Conclusions

In this work, the TSDPC strategy with neural switching table of the DFIG-DRWP was presented, and it was compared with the classical TSDPC method. The simulation results obtained for the proposed technique illustrated a considerable reduction in the THD values of the current, rotor flux ripple, reactive power ripple, torque ripple, stator current ripple, and active power ripple compared to the conventional TSDPC, and even compared to the results presented in the other recent works such as [36] and [37].

## 6. Appendix

### a. FNN algorithm

The gradient, validation checks, and learning rate of FNN algorithm are shown in Figures 22, 23, and 24, respectively.

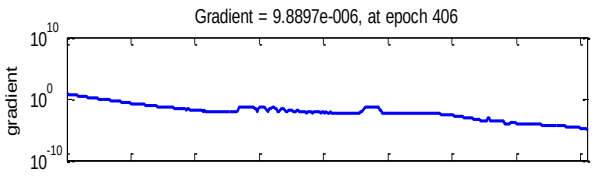


**Figure 22. Gradient.**

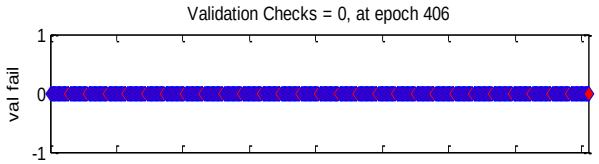


**Figure 23. Validation checks.**

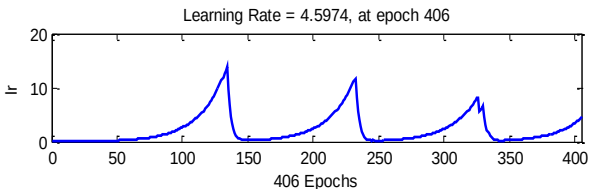


**Figure 24. Learning rate.**

## b. Model of DFIG

The modeling of DFIG used for the DPC control has been represented in the synchronous rotating reference frame as:
Rotor flux components:

$$\begin{cases} \psi_{dr} = L_r I_{dr} + M I_{dr} \\ \psi_{qr} = L_r I_{qr} + M I_{qr} \end{cases} \quad (10)$$

Stator flux components:

$$\begin{cases} \psi_{ds} = L_s I_{ds} + M I_{dr} \\ \psi_{qs} = L_s I_{qs} + M I_{qr} \end{cases} \quad (11)$$

Stator voltage components:

$$\begin{cases} V_{ds} = I_{ds} R_s - \omega_s \psi_{qs} + \dfrac{d}{dt}\psi_{ds} \\ V_{qs} = I_{qs} R_s + \omega_s \psi_{ds} + \dfrac{d}{dt}\psi_{qs} \end{cases} \quad (12)$$

Rotor voltage components:

$$\begin{cases} V_{dr} = I_{dr} R_r - \omega_r \psi_{qr} + \dfrac{d}{dt}\psi_{dr} \\ V_{qr} = I_{qr} R_r + \omega_r \psi_{dr} + \dfrac{d}{dt}\psi_{qr} \end{cases} \quad (13)$$

The stator active and reactive powers are defined as:

$$\begin{cases} P_s = \dfrac{3}{2}(V_{qs} I_{qs} + V_{ds} I_{ds}) \\ Q_s = \dfrac{3}{2}(-V_{ds} I_{qs} + V_{qs} I_{ds}) \end{cases} \quad (14)$$

The mechanical equation of the DFIG:

$$T_e - T_r = J \cdot \frac{d\Omega}{dt} + f_r \cdot \Omega \quad (15)$$

with:

$$T_e = \frac{3}{2} p \frac{M}{L_r}(I_{dr}.\psi_{qs} - I_{qr}.\psi_{ds}) \quad (16)$$

## References

[1] Hu, J., Zhu, J., Dorrell, D.G. (2015). Predictive direct power control of doubly fed induction generators under unbalanced grid voltage conditions for power quality improvement. IEEE Transactions on Sustainable Energy, Vol. 6, No. 3.

[2] Benbouhenni, H., Boudjema, Z., and Belaidi, A. (2019). Direct vector control of a DFIG supplied by an intelligent SVM inverter for wind turbine system. Iranian Journal of Electrical & Electronic Engineering, Vol. 15, No. 1, pp. 45-55.

[3] Benbouhenni, H. (2019). Application of five-level NPC inverter in DPC-ANN of doubly fed induction generator for wind power generation systems. International Journal of Smart Grid, Vol. 3, No. 3, pp. 128-137.

[4] Izanlo, A., Gholamian, S. A., and Kazemi, M.V. (2017). Comparative study between two sensorless methods for direct power control of doubly fed induction generator. Rev. Roum. Sci. Techn.-Electrotechn. Et Energ, Vol. 62, No. 4, pp. 358-364.

[5] Benbouhenni, H. (2019). Direct power control of a DFIG fed by a seven-level inverter using SVM strategy. International Journal of Smart Grid, Vol. 3, No. 2, pp. 54-62.

[6] Kazemi, M.V., Yazdankhah, A.S., and Kojabadi, H.M. (2010). Direct power control of DFIG based on discrete space vector modulation. Renewable Energy, Vol. 35, pp. 1033-1042.

[7] Wa, Y. and Yang, W. (2016). Different control strategies on the rotor side converter in DFIG-based wind turbines. Energy Procedia, Elsevier, Vol. 100, pp. 551-555.

[8] Benbouhenni, H. (2018). Five-level DTC with 12 sectors of induction motor drive using neural networks controller for low torque ripple. Acta Electrotechnica et Informatica, Vol. 18, No. 2, pp. 61-66.

[9] Benbouhenni, H. (2018). Seven-level direct torque control of induction motor based on artificial neural networks with regulation speed using fuzzy PI controller. Iranian Journal of Electrical and Electronic Engineering, Vol. 14, No. 1, pp. 85-94.

[10] Benbouhenni, H. (2019). Seven-level NPC inverter-based neuronal direct torque control of the PMSM drives with regulation speed using neural PI controller. International Journal of Intelligent Information Systems, Vol. 8, No. 5, pp. 85-96.

[11] Benbouhenni, H., Boudjema, Z., and Belaidi, A. (2019). A novel matlab/simulink model of DFIG drive using NSMC method with NSVM strategy. International Journal of Applied Power Engineering (IJAPE), Vol. 8, No. 3, pp. 221-233.

[12] Benbouhenni, H. (2020). Intelligence hysteresis comparators for a multilevel DTC control scheme of IM drive, Majlesi Journal of Mechatronic Systems. Vol. 9, No. 2, pp. 15-21.

[13] Benbouhenni, H., Boudjema, Z., and Belaidi, A. (2018). Neuro-second order sliding mode control of a DFIG supplied by a two-level NSVM inverter for wind turbine system. Iranian Journal of Electrical & Electronic Engineering, Vol. 14, No. 4, pp. 362-373.

[14] Benbouhenni, H., Boudjema, Z., and Belaidi, A. (2019). Using four-level NSVM technique to improve DVC control of a DFIG based wind turbine systems. Periodica Polytechnica Electrical Engineering and Computer Science, Vol. 63, No. 3.

[15] Benbouhenni, H. (2018). Comparative study between NSVM and FSVM strategy for a DFIG-based wind turbine system controlled by neuro-second order sliding mode. Majlesi Journal of Mechatronic Systems, Vol. 7, No. 1, pp. 33-43.

[16] Benbouhenni, H. (2019). Sliding mode with neural network regulateur for DFIG using two-level NPWM strategy. Iranian Journal of Electrical & Electronic Engineering, Vol. 15, No. 3, pp. 411-419.

[17] Benbouhenni, H., Boudjema, Z., and Belaidi, A. (2019). Power ripple reduction of DPC DFIG drive using ANN controller. Acta Electrotechnica et Informatica, Vol. 20, No. 1, pp. 15-22.

[18] Benbouhenni, H. (2018). A new SVM scheme based on ANN controller of a PMSG controlled by DPC strategy. Majlesi Journal of Energy Management, Vol. 7, No. 1, pp. 11-19.

[19] Benbouhenni, H. (2018). Rotor flux and torque ripples minimization for direct torque control of DFIG by NSTSM algorithm. Majlesi Journal of Energy Management, Vol. 7, No. 3.

[20] Tiwari, R. and Babu, N.R. (2019). Artificial neural network-based control strategies for PMSG-based grid connected wind energy conversion system. International Journal of Materials and Product Technology, Vol. 58, No. 4, pp. 323-341.

[21] Benbouhenni, H., Boudjema, Z., and Belaidi, A. (2020). Twelve-sector DPC control based on neural hysteresis comparators of the DFIG integrated to wind power. International Journal of Smart Grid, Vol. 4, No. 1.

[22] Yaichi, I., Semmah, A., and Wira, P. (2019). Direct Power Control of a Wind Turbine based on Doubly Fed Induction Generator. European Journal of Electrical Engineering, Vol. 21, No. 5, pp. 457-464. https://doi.org/10.18280/ejee.210508.

[23] Benbouhenni, H. (2017). Hybrid neural sliding mode control of a DFIG speed in wind turbines. Majlesi Journal of Energy Management, Vol. 6, No. 4, pp. 31-41.

[24] Yahdou, A., Hemici, B., and Boudjema, Z. (2015). Sliding mode control of dual rotor wind turbine system. The mediternanean Journal of Measurement and Control, Vol. 11, No. 2, pp. 412-419.

[25] Yahdou, A., Hemici, B., and Boudjema, Z. (2015). Second-order sliding mode control of a dual-rotor wind turbine system by employing a matrix converter. Journal of Electrical Engineering, Vol. 16, No. 3, pp. 1-11.

[26] Xiong, P. and Sun, D. (2016). Backstepping-based DPC Strategy of a Wind Turbine-Driven DFIG under Normal and Harmonic Grid Voltage," in IEEE Transactions on Power Electronics, Vol. 31, No. 6, pp. 4216-4225. DOI: 10.1109/TPEL.2015.2477442.

[27] Huang, Q. and Cui, L. (2019). Design and application of face recognition algorithm based on improved backpropagation neural network. Revue d'intelligence artificielle. Vol. 33, No. 1, pp. 25-32. https://doi.org/10.18280/ria.330105.

[28] Benbouhenni, H. (2019). Comparison study between SVPWM and FSVPWM strategy in fuzzy second-order sliding mode control of a DFIG-based wind turbine. Carpathian Journal of Electronic and Computer Engineering, Vol. 12, No. 2, pp. 1-10.

[29] Benbouhenni, H., Boudjema, Z., and Belaidi, A. (2019). Higher control scheme using neural second order sliding mode and ANFIS-SVM strategy for a DFIG-based wind turbine. International Journal of Advances in Telecommunications, Electrotechnics, Signals and Systems, Vol. 8, No. 2, pp. 17-28.

[30] Yusoff, N. A., Razali, A. M., Karim, K. A., Sutikno, T., and Jidin, A. (2017). A Concept of Virtual-Flux Direct Power Control of Three-Phase AC-DC Converter. International Journal of Power Electronics and Drive System (IJPEDS), Vol. 8, No. 4, pp. 1776-1784. DOI: 10.11591/ijpeds.v8i4.pp1776-1784.

[31] Amrane, F., Chaiba, A., Babes, B.E., and Mekhilef, S. (2016). Design and implementation of high performance field oriented control for grid-connected doubly fed induction generator via hysteresis rotor current controller. *Rev. Roum. Sci. Techn.-Electrotechn. Et Energ,* Vol. 61, No. 4, pp. 319-324.

[32] Benbouhenni, H., Boudjema, Z., Belaidi, A. (2021). Direct power control with NSTSM algorithm for DFIG using SVPWM technique. Iranian Journal of Electrical & Electronic Engineering, Vol. 17, No. 2.

[33] Djeriri Y., Meroufel A., Belabbes, B., and Massoum A. (2013). Three-level NPC voltage source converter based direct power control of the doubly fed induction generator at low constant switching frequency. Revue des Energies Renouvelables, Vol. 16, No. 1, pp. 91-103.

[34] Benbouhenni, H. (2019). A direct power control of the doubly fed induction generator based on the three-level NSVPWM technique. International Journal of Smart Grid, Vol. 3, No. 4.

[35] Benbouhenni, H. (2018). Comparative Study between direct vector control and fuzzy sliding mode controller in three-level space vector modulation

inverter of reactive and active power command of DFIG-based wind turbine systems. International Journal of Smart Grid, Vol. 2, No. 4, pp. 188-196.

[36] Fayssal, A. and Azeddine, C. (2016). A novel direct power control for grid-connected doubly fed induction generator based on hybrid artificial intelligent control with space vector modulation. *Rev. Roum. Sci. Techn.-Electrotechn. Et Energ,* Vol. 61, No. 3, pp. 263-268.

[37] Naïma, M. and Mohamed-Saïd, N. (2017). Direct s-power control for a doubly fed induction generator. *Rev. Roum. Sci. Techn.-Electrotechn. Et Energ,* Vol. 62, No. 4, pp. 365-370.